

## Instability of Baroclinic Tidal Flow in a Stratified Fjord

ZHIYU LIU\*

*School of Ocean Sciences, Bangor University, Anglesey, United Kingdom, and Physical Oceanography Laboratory, Ocean University of China, Qingdao, China*

(Manuscript received 25 September 2008, in final form 16 July 2009)

### ABSTRACT

The Taylor–Goldstein equation is used to investigate the stability of a baroclinic tidal flow observed in a stratified fjord. The flow is analyzed at hourly intervals when turbulent dissipation measurements were made. The critical gradient Richardson number is often close to the Miles–Howard limit of 0.25, but sometimes it is substantially less. Although during 8 of the 24 periods examined the flow is marginally stable, it is either very stable or very unstable in others. For the unstable flow, the  $e$ -folding period of the fastest growing disturbances is 83–455 s, about 46% of the buoyancy period at the levels where the fastest growing disturbances have their maximum amplitude. These disturbances to the flows have wavelengths about 20%–72% of the water depth and have mostly a second-mode structure. Simultaneous measurements of the flow and turbulence allow for testing of the hypothesis that the growth rates of the most unstable disturbances are related to the turbulent dissipation rates. Dissipation is found to depend on the growth rates, but only to a power of about 1.2; there is a stronger (power 1.8) dependence on the buoyancy frequency.

### 1. Introduction

Turbulent mixing caused by dynamic instability is of great importance to the vertical exchanges of momentum, mass, and heat in the stratified oceans, especially in the shelf seas where tidal and wind-forced flows are very strong.

Parameterizations of turbulent mixing in the stratified ocean interior have been devised to represent the rate of dissipation of turbulent kinetic energy per unit mass  $\varepsilon$ , by, for example, Gregg (1989), Kunze et al. (1990), Polzin et al. (1995), and MacKinnon and Gregg (2003, 2005). These parameterizations are based on the assumption that turbulence is caused by instability resulting from the shear and strain induced by internal waves. In this study, we develop this idea by examining whether  $\varepsilon$  is related to the location and rate of growth of unstable disturbances in a flow in which internal waves are present;

we test the hypothesis that a mechanistic link exists between the measured rate of dissipation of turbulent kinetic energy and the dynamic instability of the flow.

The stability characteristics of observed flows described in section 2 are found by solving the Taylor–Goldstein (T–G) equation with their measured velocity and density profiles. The method of analysis is described in section 3a and demonstrated in section 3b in a detailed examination of the flow in one period. We test the hypothesis in section 4b. This is followed by conclusions in section 5. Some details of the methodology of the stability analysis are provided in the appendix.

### 2. The data

#### a. Measurement methods

The data analyzed in this study were collected in July 2002 in the Clyde Sea (Fig. 1), which is connected to the North Channel of the Irish Sea through a sill, the “Great Plateau,” of about 40-m depth. Observations were made for 24 h at a mooring station C2 (55°21'N, 5°4'W), which is just inside the entrance sill to the fjord and where the mean water depth is 58 m. The tidal range was 2.0 m during the observational period. Velocity structure was measured with a bottom-mounted 300-kHz ADCP. A

---

\* Current affiliation: State Key Laboratory of Marine Environmental Science, Xiamen University, Xiamen, China.

---

*Corresponding author address:* Dr. Zhiyu Liu, State Key Laboratory of Marine Environmental Science, Xiamen University, 422 Siming South Road, Xiamen 361005, China.  
E-mail: zyliau@xmu.edu.cn

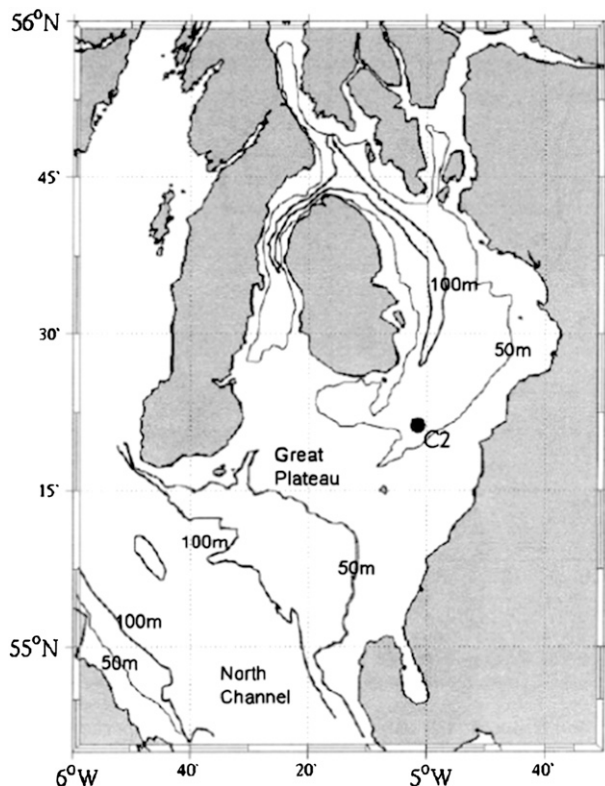


FIG. 1. The Clyde Sea and the mooring station C2.

10-min averaged velocity was obtained throughout most of the water column, 3.6–51.6 m above the seabed, with a vertical interval of 2.0 m. A free-falling microstructure Fast Light Yo-yo (FLY) profiler measured the temperature, conductivity (for salinity), and microscale velocity shear used to determine the turbulent dissipation rate through the water column (e.g., Simpson et al. 1996). The hourly deployments of FLY consisted of six consecutive casts to make the burst-averaged data statistically more robust. The interval between individual casts was 2–3 min, and the vertical resolution for the buoyancy frequency and turbulent dissipation rate is 1.0 m.

Hourly mean profiles of temperature, salinity, and turbulent dissipation rate are obtained by averaging the measurements from each hourly set of six FLY casts, which usually lasted 12–18 min, and velocity profiles were obtained for the same period, giving a set of data profiles at hourly intervals. These are used to determine  $N(z)$  and the  $[u(z), v(z)]$  eastward and northward components of velocity. For presentation simplicity, in the following sections the hourly profiles are referred to as hour-0 data through hour-24 data. Because of a mechanical failure of the FLY, no data are available for hour 20, leaving 24 sets of data for analysis.

### b. The mean flow, stratification, and dissipation

The mean (24-h averaged) stratification is characterized by a diffuse pycnocline (Fig. 2a). The mean flow is weak ( $\leq 0.05 \text{ m s}^{-1}$ ) in the lower  $\sim 30 \text{ m}$  of the water column, but it gradually increased upward to  $\sim 0.16 \text{ m s}^{-1}$  at  $z = 51.6 \text{ m}$  (Fig. 2c). As shown in Fig. 3b, the gradient Richardson number  $Ri$  of the 24-h averaged flow exceeds 0.25 everywhere; therefore, according to the Miles–Howard theorem (Miles 1961; Howard 1961), the mean flow is stable to small disturbances. Typical of wind-forced and tidally energetic flows near the upper and lower boundaries in shelf seas (e.g., Simpson et al. 1996; Rippeth and Inall 2002; MacKinnon and Gregg 2003),  $\epsilon$  decreases locally with distance from the sea surface and height above the seabed (Fig. 3c). There is some indication of an inverse relationship between  $Ri$  and  $\epsilon$ , but the correlation coefficient is not statistically significant.

### c. The variations of flow, stratification, and dissipation

The flow is dominated by the rotating semidiurnal tidal current, and the phase of the velocity varies with height from the seabed (Figs. 4b,c). High shears are located near the sea surface and in the pycnocline (cf. Figs. 4d,e), and the existence of internal tidal waves is most evident in the  $\sigma_\theta = 25.2$  and  $25.4$  isopycnals in Fig. 4d. Values of  $Ri < 0.25$  (i.e.,  $Ri^{-1} > 4$ ) are found during most of the 24-h observational period (Fig. 5a), except hour 18 and hour 19 (Fig. 5b), leaving 22-h periods of possible instability, although it may not necessarily occur;  $Ri < 0.25$  is a necessary, but not sufficient, condition for instability.

As is typical of tidally energetic stratified shelf seas, large values of  $\epsilon$  are located in three regions: near sea surface, near seabed, and in the pycnocline. The near-bottom dissipation exhibits a strong quarter-diurnal variation as found by, for example, Simpson et al. (1996) and Liu et al. (2009). Low dissipations ( $\epsilon < 10^{-8} \text{ W kg}^{-1}$ ) are located in the layer between the pycnocline and the tidal bottom boundary layer (the blue band in Fig. 5c), where  $Ri$  is almost always more than 0.25 (i.e.,  $Ri^{-1} < 4$ , in gray in Fig. 5a); however, (comparing Figs. 5c, 4d) the tidal variation in height of the pycnocline is seen to be linked to the variations of the dissipation. The time-height variations of  $Ri^{-1}$  and  $\log_{10}\epsilon$  (Figs. 5a,c) show a generally inverse relationship between  $Ri$  and  $\epsilon$ , but the correlation coefficient between  $Ri^{-1}$  and  $\log_{10}\epsilon$  varies with depth. It is, for instance, not statistically significant near the sea surface and at  $z = 19\text{--}24 \text{ m}$ ; is about 0.50 [with 95% confidence interval (CI) being 0.12–0.75] at  $z = 8\text{--}16 \text{ m}$ ; and is up to 0.92 (95% CI,

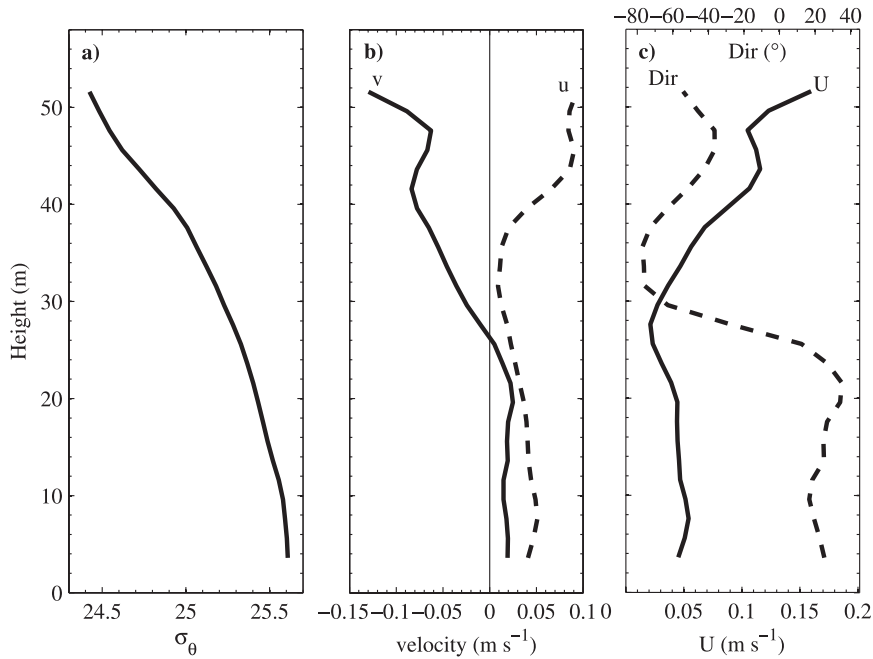


FIG. 2. Ensemble averaged profiles over 24 h of (a) the potential density  $\sigma_\theta$ , (b) the eastward component  $u$  and the northward component  $v$ , and (c) the magnitude  $U$  and direction  $Dir$ , measured counterclockwise from east, of the flow.

0.82–0.97) at  $z = 30$  m. The correlation coefficient between the pycnocline-averaged values of  $Ri^{-1}$  and  $\log_{10}\epsilon$ , defined as the average at the heights between the

two isopycnals,  $\sigma_\theta = 25.0$  and  $25.4$ , in Fig. 5c, is found to be 0.68 (95% CI, 0.38–0.85), indicative of a relatively weak local physical connection between flow stability and  $\epsilon$ .

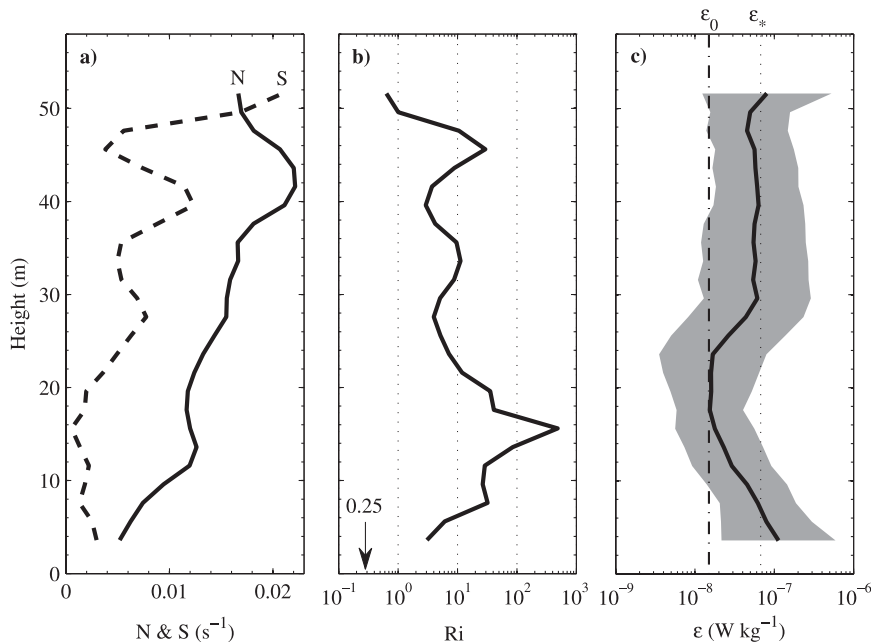


FIG. 3. The (a) buoyancy frequency  $N$  and shear  $S$  of the mean flow over 24 h, (b) the gradient Richardson number  $Ri$ , and (c) the turbulent dissipation rate  $\epsilon$ . The mean  $\pm$  standard deviation ranges of  $\epsilon$  are shaded in (c), and values of  $\epsilon_*$  and  $\epsilon_0$  are shown as dotted and dashed–dotted lines. See text for details.

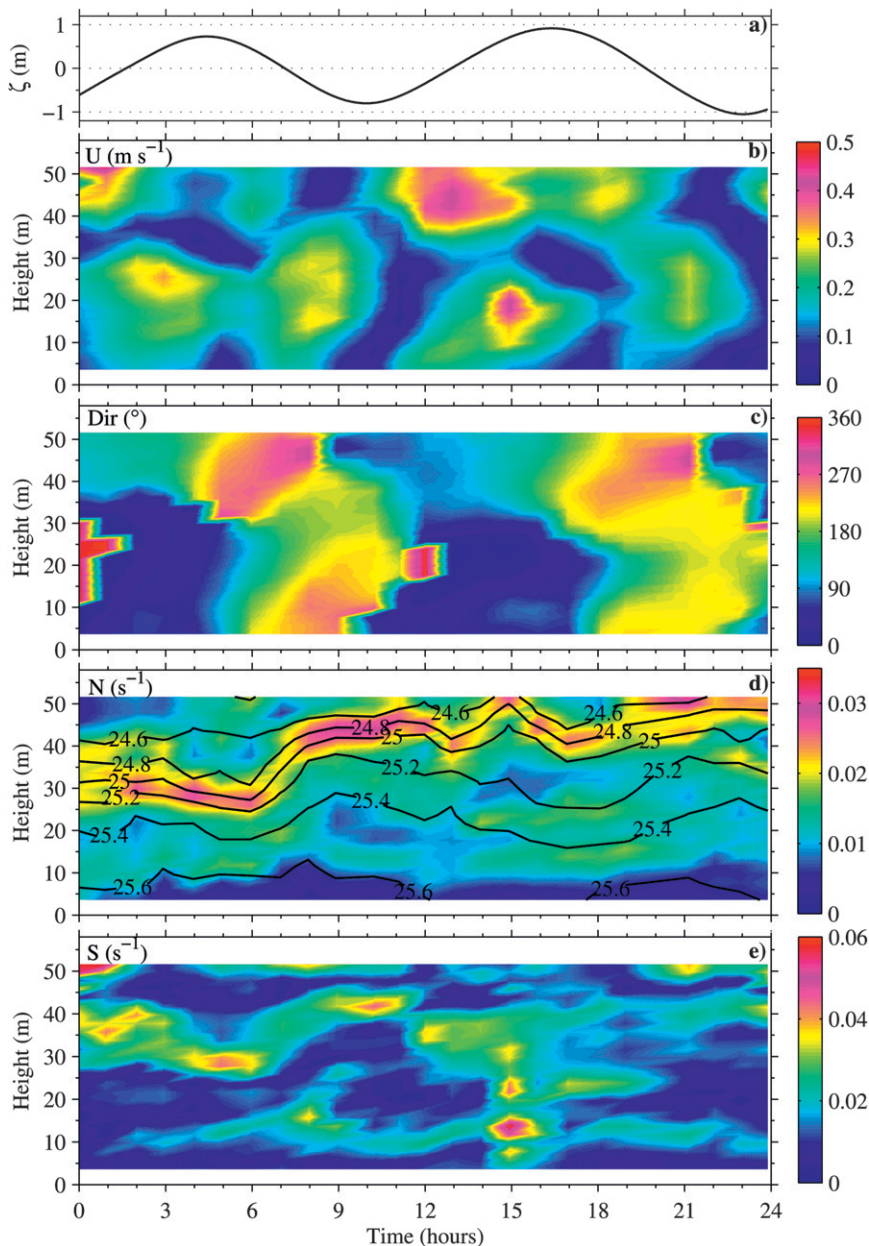


FIG. 4. The time variations of (a) the surface elevation  $\zeta$ , (b) the magnitude  $U$  and (c) direction  $\text{Dir}$  of the velocity, (d) the buoyancy frequency  $N$ , and (e) the shear  $S$  over the 24-h period. The marked contours of the potential density  $\sigma_\theta$  are overlaid to the image plot of  $N$  to better indicate the variation of the pycnocline.

### 3. Analytical methodology

#### a. The Taylor–Goldstein equation and its numerical solution

The stability of an inviscid, incompressible, stably stratified, Boussinesq shear flow to small disturbances is determined by the solutions of the T–G equation

$$\phi'' + \left[ \frac{N^2}{(U - c)^2} - \frac{U''}{U - c} - k^2 \right] \phi = 0, \quad (1)$$

where  $\phi(z)$  is the  $z$ -dependent amplitude of the streamfunction of a disturbance with real horizontal wave-number  $k$  and complex phase speed  $c (=c_r + ic_i)$ ,  $\phi'' = d^2\phi/dz^2$ , and  $U(z)$  and  $N(z)$  are the profiles of velocity

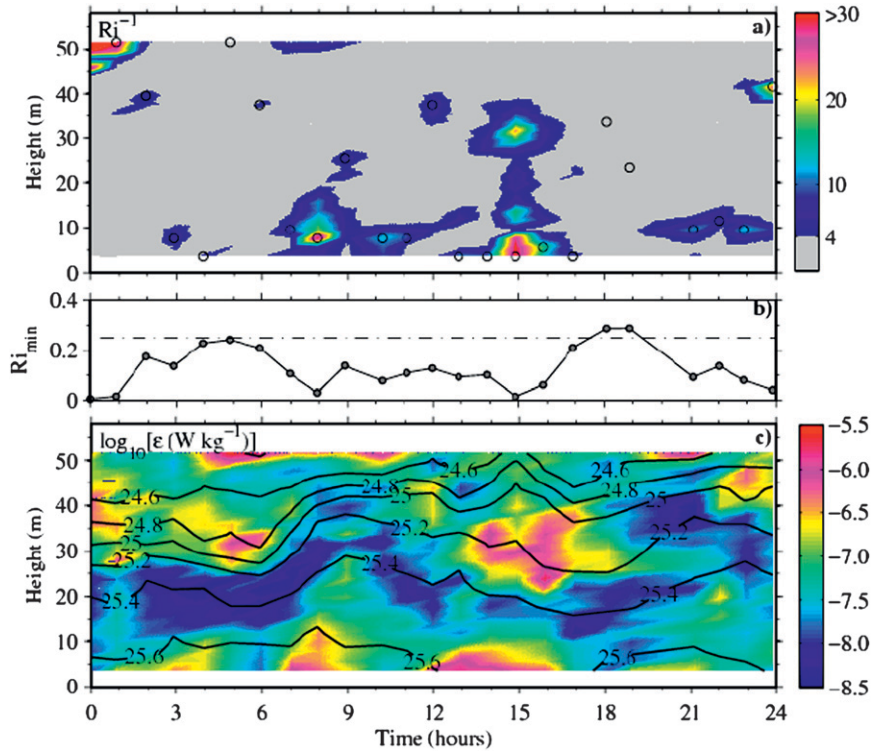


FIG. 5. The time variations of (a) the inverse gradient Richardson number  $Ri^{-1}$ , (b) the minimum  $Ri$  in the flow  $Ri_{min}$ , and (c) the turbulent dissipation rate  $\epsilon$  over 24 h. The dashed-dotted line in (b) shows a critical value of 0.25. No data are available for hour 20 as a result of a mechanical failure of FLY. The levels at which  $Ri_{min}$  is located are indicated by solid circles in (a). The marked contours of the potential density  $\sigma_\theta$  are overlaid to show the position of the pycnocline in (c).

and buoyancy frequency;  $U'' = d^2U/dz^2$ . Solutions with  $kc_i > 0$  grow exponentially in time. The flow is then unstable to shear or Kelvin–Helmholtz instability. Two Dirichlet boundary conditions of (1) are adopted: the vertical velocity and therefore  $\phi(z)$  are zero at horizontal rigid boundaries,  $z = 0$  the seabed and  $z = h$  the sea surface. The stability of two-dimensional disturbances to nonparallel flows can be examined by taking  $U$  as the velocity component in the direction of the disturbance wave vector (e.g., Sun et al. 1998; Thorpe 1999).

The T–G equation can be numerically solved via a standard shooting method (e.g., Thorpe and Jiang 1998) or a matrix method (Monserrat and Thorpe 1996). The matrix method can find all the modes of disturbances given a sufficiently fine vertical resolution of the velocity and density profiles, whereas the shooting method often misses some modes, including even the fastest growing mode. We therefore use the matrix method in this study. It is found that results obtained from the two methods generally agree to within 3%, therefore validating the general usefulness of the matrix method. As in Thorpe and Liu (2009), we shall analyze the hourly mean data

including, as it does, the effects of internal waves and turbulence; our estimates of, for example, growth rates relate to disturbances to the flow, including these effects.

*b. Stability analysis*

We choose hour 15 to demonstrate the stability analysis in some detail. Although not typical, it is evidently a period with a pronounced “signal” of low  $Ri$  and high dissipation. It is later found to have the greatest growth rate.

As shown in Figs. 6a,b, both of the two velocity components show a pronounced baroclinic structure, and the stratification is characterized by a diffuse pycnocline. From  $z = \sim 39$  m to the sea surface,  $Ri$  is always more than 0.25, but the buoyancy frequency is substantially less than the shear in the lower  $\sim 39$  m of the water column, with  $Ri < 0.25$  (Figs. 6c,d). The turbulent dissipation rate  $\epsilon$  shows a gradual decrease with the height from the seabed in the lower 20 m of the water column, indicating a pronounced bottom boundary layer (Fig. 6e). Above this layer, the variation of  $\epsilon$  shows an inverse relationship with that of  $Ri$  (cf. Figs. 6d,e); the correlation coefficient between  $Ri^{-1}$  and  $\log_{10}\epsilon$  is 0.52 (95% CI, 0.03–0.81).

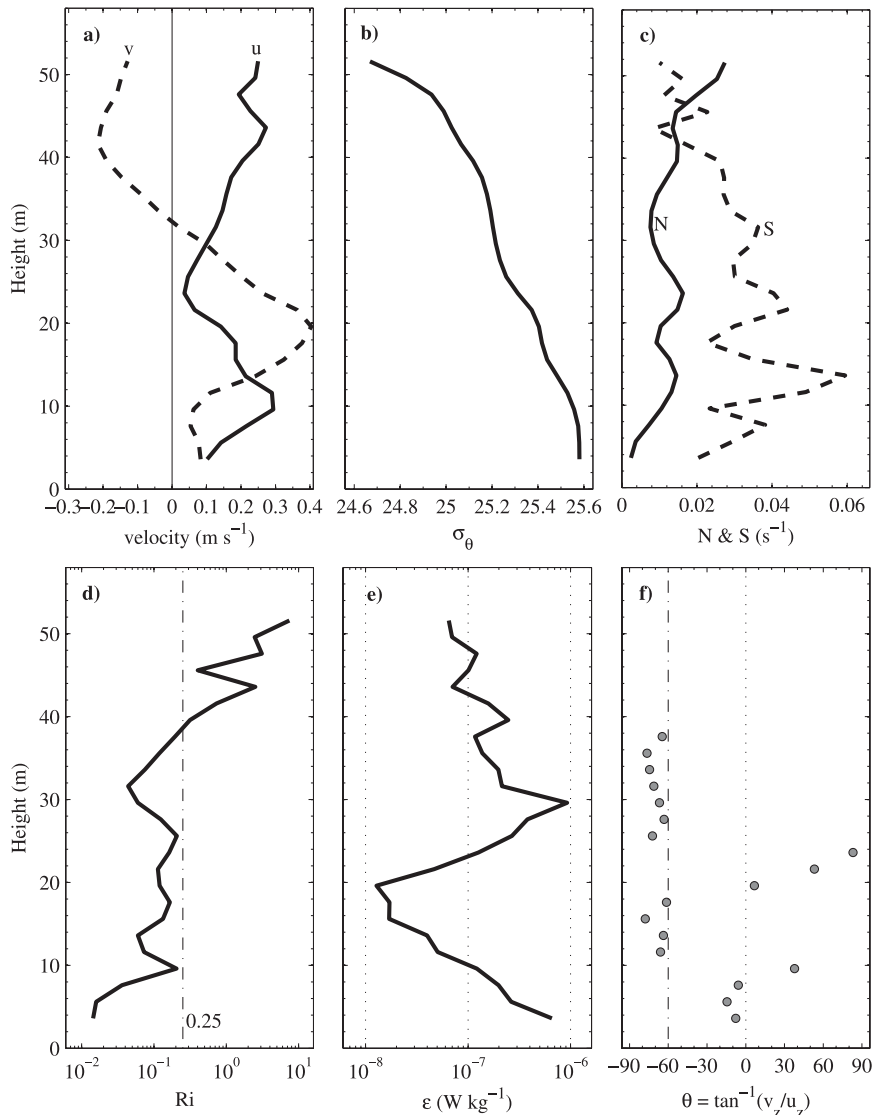


FIG. 6. Profiles of (a) the velocity components  $u$  and  $v$ , (b) the potential density  $\sigma_\theta$ , (c) the shear  $S$  and the buoyancy frequency  $N$ , (d) the gradient Richardson number  $Ri$ , (e) the turbulent dissipation rate  $\epsilon$ , and (f) the direction of shear  $\theta$  in the region  $Ri < 0.25$  of hour 15.

Figure 6f shows that the direction of the shear in the region where  $Ri < 0.25$  is mostly in the vicinity of  $\theta = -60^\circ$ . We may therefore expect that the fastest growing disturbances to the flow may propagate in a direction near  $\theta = -60^\circ$ .

### 1) STABILITY CHARACTERISTICS

Following Sun et al. (1998) and Thorpe (1999), the stability of two-dimensional wavelike disturbances in direction  $\alpha$  are examined by replacing the velocity in the T-G equation with the velocity component  $U_\alpha = u \cos \alpha + v \sin \alpha$ , where  $u$  and  $v$  are the eastward and

northward components of the velocity vector, respectively, and  $\alpha$  is the direction of the disturbance wave vector measured counterclockwise from the eastward direction of  $u$ . By taking advantage of the symmetry of the T-G equation in  $\pm k$ , only half of the wave vector space needs to be covered in the analysis. We choose  $\alpha$  to be in the range of  $-90^\circ$  to  $90^\circ$ , with a  $5^\circ$  increment in the analysis; that is, the velocity vector is projected to 37 evenly distributed directions between  $-90^\circ$  and  $90^\circ$ . Stability is assured by the Miles-Howard theorem if the directional gradient Richardson number  $Ri_\alpha = N^2 / (\partial U_\alpha / \partial z)^2$  is more than 0.25 for all  $z$ . We therefore do not seek unstable disturbances in these directions.

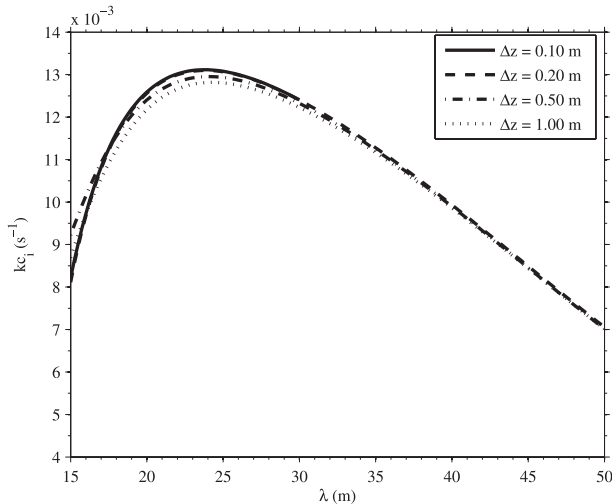


FIG. 7. The growth rate vs wavelength plot for mode 1 using hour-15 flow with four different grid sizes. A narrower wavelength range is shown to emphasize the effect of the grid size on the fastest growing disturbances.

For other values of  $\alpha$ , the T–G equation is numerically solved with a range of horizontal wavenumber  $k$ . Recognizing that it is not clear what wavenumber range should be used in the calculation, we tried a very large range of wavenumber (wavelength) for a few of the 1-h flows before defining an appropriate range of wavenumber for the stability analysis. It is found that a wavelength range of 0.5–60 m covers all the wavelengths of the fastest growing disturbances to the flows examined, and we adopt this range in all the subsequent calculations.

Velocity and  $N^2$  profiles with relatively fine resolution are needed to solve the T–G equation precisely using the matrix method. We interpolate velocity and  $N^2$  profiles from their observed values at 2- and 1-m vertically spaced levels, respectively, to evenly spaced grids of 0.20-m size. A linear interpolation method is used for  $N^2$ , whereas a cubic spline interpolation is conducted for the velocity profile noting that second-order derivatives are needed in the T–G equation. Sensitivity to the grid size ( $\Delta z$ ) is studied by conducting the calculations for the same velocity and  $N^2$  profiles with different grid sizes. As shown in Fig. 7, the growth rate versus wavelength plot for mode 1 using hour-15 flow with four different grid sizes, the results converge with decreasing  $\Delta z$ . The greatest growth rate increases as  $\Delta z$  decreases, but (by interpolation) a finer resolution would result in a difference of less than 1% when a size of 0.20 m is used; both the greatest growth rate and corresponding wavelength are almost identical for grid sizes of 0.20 and 0.10 m.

In some hourly periods, the layer of low  $Ri$  ( $<0.25$ ) is very thin, with only one point of the original data having

a value of  $Ri$  less than 0.25. Estimates of the greatest growth rates by directly solving the T–G equation then become unreliable. We therefore test whether the results of the stability analysis converge with decreased vertical interval  $\Delta z$ , setting a threshold that, within 1%, the greatest growth rates are independent—that is, the changes of the growth rates are less than the threshold—of  $\Delta z$  once a relatively fine resolution—for example, 0.20 m—is achieved. Only seven cases pass this threshold condition.

Further results of analyzing the hour-15 data are shown in Figs. 8–10. There are always regions in which the  $Ri_\alpha$  is less than 0.25 (Fig. 8a), suggesting the possible existence of unstable disturbances in all the directions. The fastest growing disturbance is found to propagate in direction  $\alpha = -60^\circ$ , with a wavelength of 24.0 m and a growth rate of  $1.31 \times 10^{-2} \text{ s}^{-1}$  (Fig. 8b). The flow is generally most unstable to the second mode (Fig. 9), defined by number of the zero crossings of the streamfunction, with maxima of the amplitude of the streamfunction being near positions where  $Ri_\alpha$  has a minimum (cf. Figs. 8a, 9). The fastest growing disturbance has a second-mode vertical structure, with the maximum amplitude of the streamfunction (and also vertical velocity) at a height of 14.2 m and the second maxima at 9.8 m (Fig. 10a). The direction  $\alpha = -60^\circ$  is that of the shear in this vicinity (see Fig. 6f), although the flow (Fig. 6a) is toward the northeast:  $\alpha \approx 45^\circ$ . (Notice that the definition of  $\alpha$  is in agreement with that of  $\theta$ .) The phase speed of the fastest growing disturbance  $c_r$  is  $-0.056 \text{ m s}^{-1}$ , and it matches the mean flow  $U_\alpha(z)$  at  $z_1 = 13.0 \text{ m}$  and  $z_2 = 28.9 \text{ m}$  (Fig. 10c). The greatest growth rate of disturbances corresponds to an  $e$ -folding period of 76.3 s, about 17% of the buoyancy period at the level of the maximum in the amplitude of the streamfunction.

## 2) MARGINAL STABILITY

We examine now how unstable the flow is and whether it is marginally stable (Thorpe and Liu 2009), modifying the real mean flow  $U$  with a parameter  $\Phi$  as  $U_\Phi = (1 + \Phi)U$ , therefore increasing (or decreasing, depending on the sign of  $\Phi$ ) the velocity by a factor of  $\Phi$ . By setting a series of values for  $\Phi$ , the fastest growing disturbances (if they exist) of the modified flows are obtained by solving the T–G equation with  $U_\Phi$  and  $N^2$ , the observed buoyancy frequency squared. If the numerical method of solving the T–G equation is robust, then a critical value,  $\Phi_c$ , the “marginal stability parameter,” is found by gradually decreasing  $\Phi$  until the maximum growth rate becomes zero.

Because of the numerical errors in solving matrix eigenvalue problems, it is difficult to estimate  $\Phi_c$  directly. Unstable disturbances are sometimes found even when

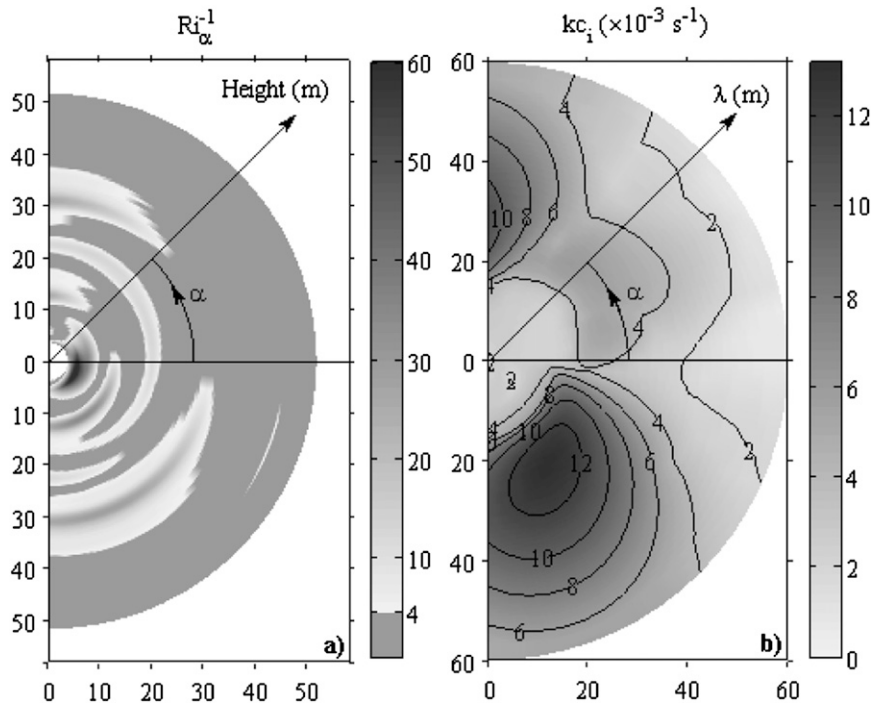


FIG. 8. The distributions of (a) the inverse directional gradient Richardson number  $Ri_{\alpha}^{-1}$  in  $z - \alpha$  space and (b) the growth rate  $kc_i$  in the wave vector space for hour 15;  $kc_i$  is shown against wavelength  $\lambda$  in (b) to demonstrate more clearly the size of the wavelength of the disturbances.

$Ri$  is more than 0.25 everywhere in the flow. To overcome this difficulty, we estimate the marginal stability parameter in an indirect way: the T-G equation is solved with the modified flows with a series of  $\Phi$ , from some lower limit at which the value determined for  $kc_i$  is small up to an upper limit value of 1. The growth rate versus  $\Phi$  relation is then extrapolated to a zero growth rate using a polynomial function. The order of the polynomial function depends on the nature of the calculated growth rate versus  $\Phi$  relation.

Figure 11a shows the maximum growth rate for hour 15 at  $\alpha = -60^\circ$  as a function of  $\Phi$ . The minimum  $Ri$ , equal to the minimum  $Ri$  that is observed divided by  $(1 + \Phi)^2$ , equals 0.25 when  $\Phi = -0.72$  and is greater than 0.25 in the shaded region where, by the Miles-Howard theorem, the flow is stable and no positive values of the growth rate  $kc_i$  are possible. A third-order polynomial closely fit the points, tending smoothly to  $\Phi_c = -0.69 \pm 0.03$  at  $kc_i = 0$ , except for very small values of the maximum growth rate where  $\Phi < -0.5$  and where the numerically estimated growth rates exceed the polynomial values and do not tend to zero even when the minimum  $Ri$  is equal to, or even greater than, 0.25.

It is expected that the growth rate should approach zero smoothly as the minimum  $Ri$  tends to its critical value, a value that must be less than or equal to 0.25.

This is indeed found by Hazel (1972), using shooting method solutions of the T-G equation for analytical forms of velocity and  $N^2$ , and it is confirmed by our solutions using the matrix method.<sup>1</sup> The discrepancy between the polynomial trend and the numerically estimated values appears to be a consequence of increasingly poor resolution in  $z$  of values of  $Ri$  less than the critical value  $Ri_c$ , the number of such points decreasing as the minimum  $Ri$  approaches  $Ri_c$ , and of the developing singularities in the T-G equation, (1), at levels where  $(U - c)$  approaches zero as the imaginary part of  $c$  (or the growth rate) tends toward zero.

An indirect estimate of the stability characteristics can be made for the 15 flows in which the growth rates are difficult to estimate precisely. For cases in which  $kc_i$  does not converge and satisfy the prescribed threshold condition as  $\Delta z$  decreases, convergence is found when  $U_{\alpha}$  is increased by a sufficiently large factor  $\Phi (>0)$ , and an

<sup>1</sup> The shooting and matrix methods give similar results, although the matrix method solutions of analytical profiles (e.g., hyperbolic tangent type profiles of velocity and density) demonstrate a similar problem to that discussed earlier as the minimum  $Ri$  tends to  $Ri_c$  from below and when  $kc_i$  is small. These tests of the matrix method solution provide a means of estimating the size of ( $\pm$ ) uncertainty in  $Ri_c$ .

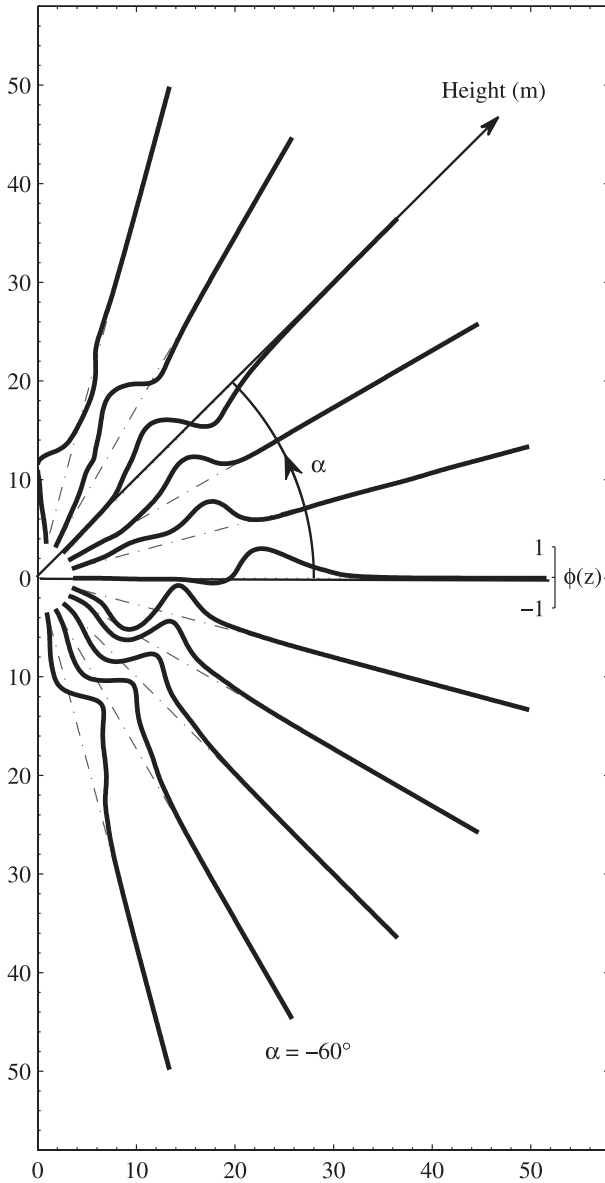


FIG. 9. The normalized amplitude of the streamfunction  $\phi(z)$  of the fastest growing disturbances in several directions for hour 15. Only the results of every  $15^\circ$  are plotted to clearly show the vertical (along each dashed-dotted line in the plot) structure of the streamfunction.

estimate of the maximum value of  $kc_i$  as  $\Phi$  tends to zero is found by extrapolation (e.g., as shown in Fig. 11b for hour 6). The shape of the streamfunction and the wavenumber of the fastest growing disturbances are generally not very sensitive to changes in  $\Phi$  between 0 and 1, so that both can also be estimated as  $\Phi$  tends to zero and hence in the observed conditions.

The marginal stability parameter  $\Phi_c = -0.69 \pm 0.03$  implies that a reduction of velocity of  $(69\% \pm 3\%)$  is required to stabilize the flow; the flow is therefore very

unstable and not “marginal” as defined by Thorpe and Liu (2009). The  $Ri_c$  of the flow is  $0.21 \pm 0.04$ , close to 0.25. The propagation direction of the fastest growing mode does not change (from  $-60^\circ$ ) as  $\Phi$  is reduced.

#### 4. Results

##### a. Maximum growth rates and marginal stability

We now apply the methodology described in section 3 to investigate the variations of dynamic instability in the 21 other hourly periods of possible instability.

Results are shown in Table 1. The maximum growth rates are  $(0.4\text{--}1.31) \times 10^{-2} \text{ s}^{-1}$ , with  $e$ -folding period  $\tau$  ranging from 0.06 to 9 times the buoyancy period  $T_b = 2\pi/N$  at the levels where the amplitude of the streamfunction is maximum. The ratio  $\tau/T_b$  generally increases as  $|\Phi_c|$  decreases. Exponential growth therefore occurs in periods comparable to those of the smallest wavelength internal waves at the level of the disturbance, and substantially less than the 42–48-min periods between the hourly groups of six FLY casts.

Values of  $\Phi_c$  and  $Ri_c$  are estimated as in section 3b. The values of  $|\Phi_c|$  are not always very much less than unity, implying that marginal instability is not always found. In nine cases,  $Ri_c$  lies between 0.21 and 0.25 and, given the uncertainty of the estimates, is indistinguishable from the Miles–Howard upper limit of 0.25 for unstable disturbances; however, in six cases, a value of the minimum  $Ri$  less than 0.1 is required before instability can occur.

##### b. Comparison with dissipation rates

We now test the hypothesis that the growth rates of the most unstable disturbances are related to the observed  $\varepsilon$ . We establish a vertical interval,  $z_1 \leq z \leq z_2$ , over which the modulus of the normalized amplitude of the streamfunction  $\phi(z)$  (proportional to the amplitude of the fastest growing disturbance) exceeds a threshold value,  $\delta$ , between 0 and 1. Then  $E = \int_{z_1}^{z_2} \varepsilon dz$ , where  $\varepsilon$  is the observed turbulent dissipation rate, provides a measure of turbulent dissipation in the region where instability is predicted to occur. Figure 12 shows the height ranges in which the integrated dissipation rates  $E$  are calculated for  $\delta = 0.2$ .

As shown in Fig. 12, the streamfunctions of the unstable disturbances are moderately successful in evaluating where large dissipations occur. A quantitative test of the hypothesis is, however, required: Is  $E$  related to the instability variables (i.e.,  $kc_i$ , the wavelength  $\lambda$ ,

<sup>2</sup> This value of  $\delta$  is later found to be an appropriate small value that can be used to test the validity of Eq. (2).

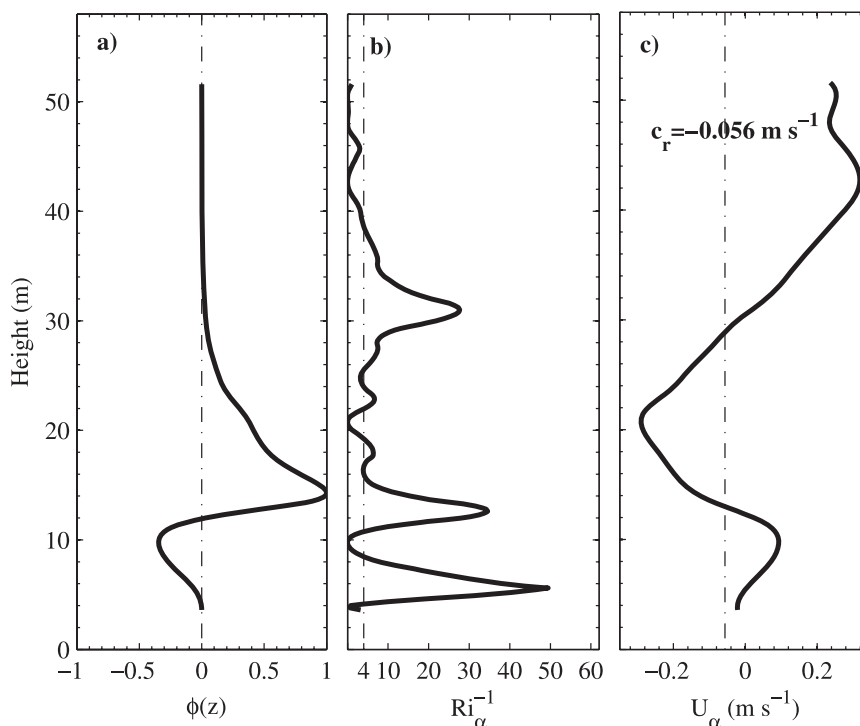


FIG. 10. The (a) amplitude of the normalized streamfunction  $\phi(z)$  of the fastest growing disturbance, (b) inverse directional gradient Richardson number  $Ri_{\alpha}^{-1}$ , and (c) velocity component in direction  $\alpha = -60^{\circ}$  for hour 15 with boundaries set at 3.6 and 51.6 m.

and the vertical range  $l$  ( $\equiv z_2 - z_1$ ) of the fastest growing disturbance)?

It is found that  $l$  and  $\lambda$  are highly correlated for small values of  $\delta$ : the correlation coefficient  $r \geq 0.82$  (95% CI, 0.53–0.94) when  $\delta \leq 0.18$ , and  $r \geq 0.66$  (95% CI, 0.22–0.88) when  $\delta \leq 0.34$ ; for small values of  $\delta$ , the wavelength  $\lambda$  is, alone, an appropriate length scale for a scaling formula of  $E$ . We, therefore, for small values of  $\delta$ , propose and test the following dimensionally correct scaling formula

$$E_L = \varepsilon_* l + c_0 (kc_i)^{3-a} N^a \lambda^3, \quad (2)$$

depending on  $kc_i$ ,  $N$  (the buoyancy frequency at the level where  $|\phi(z)|$  is maximum), and  $\varepsilon_*$  (a background turbulent dissipation rate). The  $Ri$ , or better the term that provides a measure of instability,  $(Ri - Ri_c)$  or  $\Phi_c$ , are not included in the formulation of  $E$ ; a measure of  $(Ri - Ri_c)$  is already provided by  $kc_i$ .

The three unknowns— $\varepsilon_*$ ,  $c_0$ , and  $a$ —in (2) are estimated for a range of values of  $\delta$  by best fitting to the data. It is found that  $\varepsilon_*$  and  $a$  are not sensitive to variations in  $\delta$  for  $0.12 \leq \delta \leq 0.34$ , but the proportion of midwater-integrated turbulent dissipation  $E_{\text{mid}}$ , defined as  $\int_{10\text{m}}^{47\text{m}} \varepsilon dz$ , accounted for by  $E_L$  decreases with  $\delta$ , less than 50% of  $E_{\text{mid}}$  being accounted for when  $\delta > 0.20$ .

For  $0.12 \leq \delta \leq 0.34$ ,  $\langle \varepsilon_* \rangle$  is estimated as  $(6.72 \pm 0.22) \times 10^{-8} \text{ W kg}^{-1}$ , where  $\langle \rangle$  represents mean  $\pm$  standard deviation, and  $\langle a \rangle = 1.83 \pm 0.04$ . The fairly small variance of  $\varepsilon_*$  confirms the existence of a nearly constant background turbulence. The estimates of  $a$  indicate that there is a stronger dependence of  $E$  on  $N$ , with a power of about 1.8, than on  $kc_i$  (power about 1.2). This supports Thorpe and Liu's (2009) conjecture that the growth rate of small disturbances, and hence turbulence in the flow, is largely under a physical control from the stratification. The estimated values of  $c_0$ , as expected from the form of (2), generally decrease with increased  $\delta$ , but no reliable quantitative dependence can be drawn from the present dataset.

Equation (2) represents our proposed relationship. Although a relatively high correlation coefficient, more than 0.75 (95% CI, 0.39–0.91) for  $0.12 \leq \delta \leq 0.34$ , is obtained using (2), the difference between observed and predicted values of  $E$  with the best-fit values of the unknowns ( $\varepsilon_*$ ,  $c_0$ ,  $a$ ) leads to an uncertainty factor of about 3. As implied by the wide range of 95% confidence interval, the high correlation coefficient is partly related to the low number of degrees of freedom in the comparison. More extensive datasets are required to test the validity of the formula, and, if it is valid, to make more reliable estimates of the unknowns.

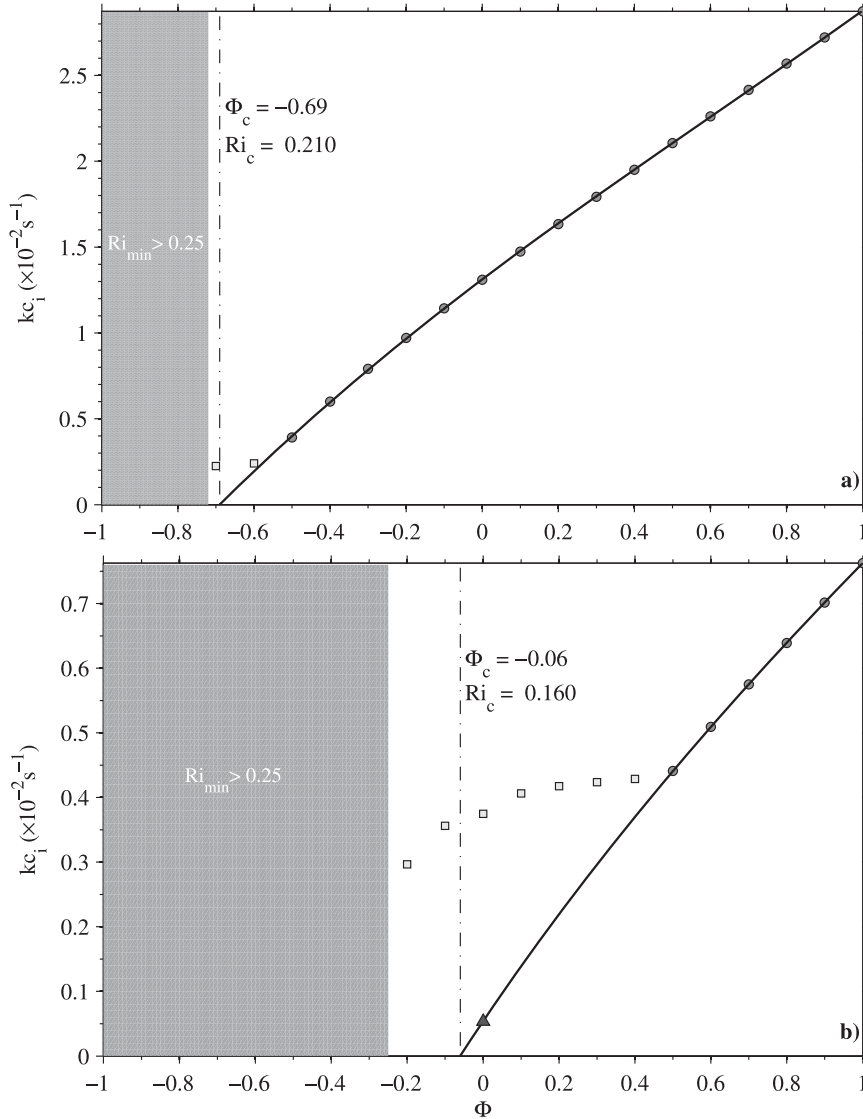


FIG. 11. The greatest growth rate  $kc_i$  vs  $\Phi$  plot of (a) hour 15 and (b) hour 6. For hour 15, a marginal stability parameter  $\Phi_c$  of  $-0.69 \pm 0.03$  is estimated based on a third-order polynomial interpolation, and the critical gradient Richardson number  $Ri_c$  of the flow is estimated to be  $0.21 \pm 0.04$ . For hour 6, the maximum growth rate, marked as a solid triangle in (b) at  $\Phi = 0$ , is estimated via interpolation, and  $\Phi_c$  and  $Ri_c$  are estimated to be  $-0.06 \pm 0.01$  and  $0.16 \pm 0.02$ , respectively.

*c. Related formula for shelf sea dissipation rates*

MacKinnon and Gregg (2003, 2005), using data from the New England shelf, propose a scaling formula for the dissipation designed  $\varepsilon_{MG}$ ,

$$\varepsilon_{MG} = \varepsilon_0 \left( \frac{N}{N_0} \right) \left( \frac{S_{lf}}{S_0} \right), \tag{3}$$

where  $S_{lf}$  is the low-frequency, low-mode resolved shear (i.e., that of the internal tide). For simplicity  $S_0$  and  $N_0$

are set to be 3 cph ( $\equiv 5.2 \times 10^{-3} \text{ s}^{-1}$ ), and  $\varepsilon_0$  equals  $6.9 \times 10^{-10} \text{ W kg}^{-1}$  to best fit their later-summer data and equals  $1.1 \times 10^{-9} \text{ W kg}^{-1}$  for the spring data. The reason for the difference is unknown. The uncertainty in the estimates appears to be a factor of 2–4 (see MacKinnon and Gregg 2005, their Fig. 11, bottom right), comparable to our factor of 3.

The data from the Clyde Sea have a distribution in an  $N$  versus shear diagram similar to that found by MacKinnon and Gregg (2003, their Fig. 13a) and MacKinnon and Gregg (2005, their Fig. 11, left), and

TABLE 1. Characteristics of the fastest growing disturbances. Here,  $\lambda$  and  $kc_i$  are respectively the wavelength and growth rate of the fastest growing disturbance, and  $N$  is the buoyancy frequency at the level where the amplitude of the streamfunction is maximum;  $\tau = (kc_i)^{-1}$  is the  $e$ -folding period of the fastest growing disturbance, and  $T_b = 2\pi N^{-1}$  is the buoyancy period at the level where the amplitude of the streamfunction is maximum. The marginal instability parameter  $\Phi_c$  and the critical Richardson number  $Ri_c$  of the flows are also listed. The values shown at hour 15\* are those discussed at the end of the appendix for a pycnocline-located disturbance. Values for the seven cases that pass the threshold condition described in section 3b(1) are in bold in the table.

Hour	Mode	$\lambda$ (m)	$kc_i$ (s <sup>-1</sup> )	$N$ (s <sup>-1</sup> )	$\tau/T_b$	$\Phi_c$	$Ri_c$
<b>0</b>	<b>2</b>	<b>11.5</b>	<b><math>1.20 \times 10^{-2}</math></b>	<b><math>4.6 \times 10^{-3}</math></b>	<b>0.06</b>	<b><math>-0.83 \pm 0.02</math></b>	<b><math>0.24 \pm 0.05</math></b>
1	2	42.0	$2.4 \times 10^{-3}$	$2.19 \times 10^{-2}$	1.45	$-0.19 \pm 0.01$	$0.01 \pm 0.005$
2	2	31.0	$1.0 \times 10^{-3}$	$1.81 \times 10^{-2}$	2.88	$-0.10 \pm 0.01$	$0.20 \pm 0.03$
3	—	—	0 (stable)	—	—	$0.06 \pm 0.01$	$0.20 \pm 0.02$
4	—	—	0 (stable)	—	—	$0.41 \pm 0.02$	$0.11 \pm 0.01$
5	1	37.5	$0.4 \times 10^{-3}$	$2.24 \times 10^{-2}$	8.92	$-0.04 \pm 0.01$	$0.24 \pm 0.03$
6	2	22.0	$0.5 \times 10^{-3}$	$1.23 \times 10^{-2}$	3.93	$-0.06 \pm 0.01$	$0.16 \pm 0.02$
7	—	—	0 (stable)	—	—	$0.21 \pm 0.02$	$0.04 \pm 0.01$
<b>8</b>	<b>3</b>	<b>31.5</b>	<b><math>6.1 \times 10^{-3}</math></b>	<b><math>1.22 \times 10^{-2}</math></b>	<b>0.32</b>	<b><math>-0.53 \pm 0.03</math></b>	<b><math>0.09 \pm 0.01</math></b>
<b>9</b>	<b>2</b>	<b>16.5</b>	<b><math>5.0 \times 10^{-3}</math></b>	<b><math>8.3 \times 10^{-3}</math></b>	<b>0.26</b>	<b><math>-0.46 \pm 0.04</math></b>	<b><math>0.21 \pm 0.03</math></b>
10	1	29.0	$0.5 \times 10^{-3}$	$2.85 \times 10^{-2}$	9.08	$-0.03 \pm 0.01$	$0.07 \pm 0.01$
11	—	—	0 (stable)	—	—	$0.01 \pm 0.01$	$0.09 \pm 0.01$
<b>12</b>	<b>2</b>	<b>39.0</b>	<b><math>4.7 \times 10^{-3}</math></b>	<b><math>1.46 \times 10^{-2}</math></b>	<b>0.50</b>	<b><math>-0.36 \pm 0.03</math></b>	<b><math>0.25 \pm 0.02</math></b>
13	1	35.0	$2.0 \times 10^{-3}$	$9.4 \times 10^{-3}$	0.75	$-0.32 \pm 0.02$	$0.24 \pm 0.02$
14	—	—	0 (stable)	—	—	$0.22 \pm 0.02$	$0.03 \pm 0.01$
<b>15</b>	<b>2</b>	<b>24.0</b>	<b><math>1.31 \times 10^{-2}</math></b>	<b><math>1.40 \times 10^{-2}</math></b>	<b>0.17</b>	<b><math>-0.69 \pm 0.03</math></b>	<b><math>0.21 \pm 0.04</math></b>
<b>15*</b>	<b>2</b>	<b>47.0</b>	<b><math>5.0 \times 10^{-3}</math></b>	<b><math>8.9 \times 10^{-3}</math></b>	<b>0.28</b>	—	—
<b>16</b>	<b>2</b>	<b>16.5</b>	<b><math>4.0 \times 10^{-3}</math></b>	<b><math>1.09 \times 10^{-2}</math></b>	<b>0.44</b>	<b><math>-0.42 \pm 0.02</math></b>	<b><math>0.23 \pm 0.02</math></b>
17	—	—	0 (stable)	—	—	$0.00 \pm 0.01$	$0.23 \pm 0.02$
21	2	42.0	$2.0 \times 10^{-3}$	$6.0 \times 10^{-3}$	0.48	$-0.36 \pm 0.02$	$0.22 \pm 0.02$
22	2	26.5	$0.5 \times 10^{-3}$	$1.23 \times 10^{-2}$	3.92	$-0.10 \pm 0.02$	$0.20 \pm 0.02$
23	—	—	0 (stable)	—	—	$0.14 \pm 0.01$	$0.06 \pm 0.01$
<b>24</b>	<b>3</b>	<b>23.0</b>	<b><math>5.3 \times 10^{-3}</math></b>	<b><math>8.5 \times 10^{-3}</math></b>	<b>0.25</b>	<b><math>-0.52 \pm 0.02</math></b>	<b><math>0.12 \pm 0.01</math></b>

fits (3) with a value of  $\varepsilon_0 = 1.5 \times 10^{-8} \text{ W kg}^{-1}$ . This value of  $\varepsilon_0$  is an order larger than that obtained by MacKinnon and Gregg (2003, 2005). Although it is not clear what process is responsible for the difference in  $\varepsilon_0$ , a value of  $4.4 \times 10^{-9} \text{ W kg}^{-1}$ , closer to our estimate, is obtained by Palmer et al. (2008)<sup>3</sup> using data from the Celtic Sea, and a value of  $4.5 \times 10^{-8} \text{ W kg}^{-1}$ , almost two orders larger than MacKinnon and Gregg's values, is obtained by Sundfjord et al. (2007) with data from the marginal ice zone of the Barents Sea. This may suggest that  $\varepsilon_0$ , the energy density of the small-scale “test waves” (MacKinnon and Gregg 2003), is highly related to the hydrodynamic and topographic characteristics of the studied site.

As shown in Fig. 3c, the assumed depth-independent background turbulent dissipation rate  $\varepsilon_*$  approximately equals the tidally averaged turbulent dissipation rate in the pycnocline, whereas  $\varepsilon_0$  coincides with the minimum-averaged dissipation rate in the water column. This may indicate the physical difference between the two con-

stant dissipation rates assumed in Eqs. (2) and (3): the former represents the turbulence level in the pycnocline when there are no growing disturbances leading to dynamic instability, whereas the later, selected to make the modeled dissipation rate with (3) have the same average value as the observed data, more closely represents a background on which the low frequency waves (the baroclinic tidal waves) are superimposed.

## 5. Conclusions

In this paper we have investigated the dynamic stability of a baroclinic tidal flow observed in a stratified fjord. The principal results are as follows.

- 1) The observed flow is sometimes found to be stable to Kelvin–Helmholtz instability with a minimum  $Ri$  greater than 0.25, but it mostly has a minimum  $Ri$  less than 0.25.
- 2) The  $Ri_c$  of the observed flow is often approximately 0.25 (e.g., hours 0, 5, 12), but sometimes it is substantially less than 0.25 (e.g., hours 1, 3).
- 3) Of the 22 hourly flows with a minimum  $Ri$  less than 0.25, 4 are found to be very stable, that is,  $\Phi_c > 0$  and  $|\Phi_c|$  is not much less than unity; 8 in a state of marginal stability, that is,  $|\Phi_c| \ll 1$ ; and 10 very unstable,

<sup>3</sup> Noting that  $S_0 = N_0 = 6 \text{ cph}$  are adopted in Palmer et al. (2008), their reported value of  $\varepsilon_0$  ( $1.75 \times 10^{-8} \text{ W kg}^{-1}$ ) is divided by 4 for the present comparison.

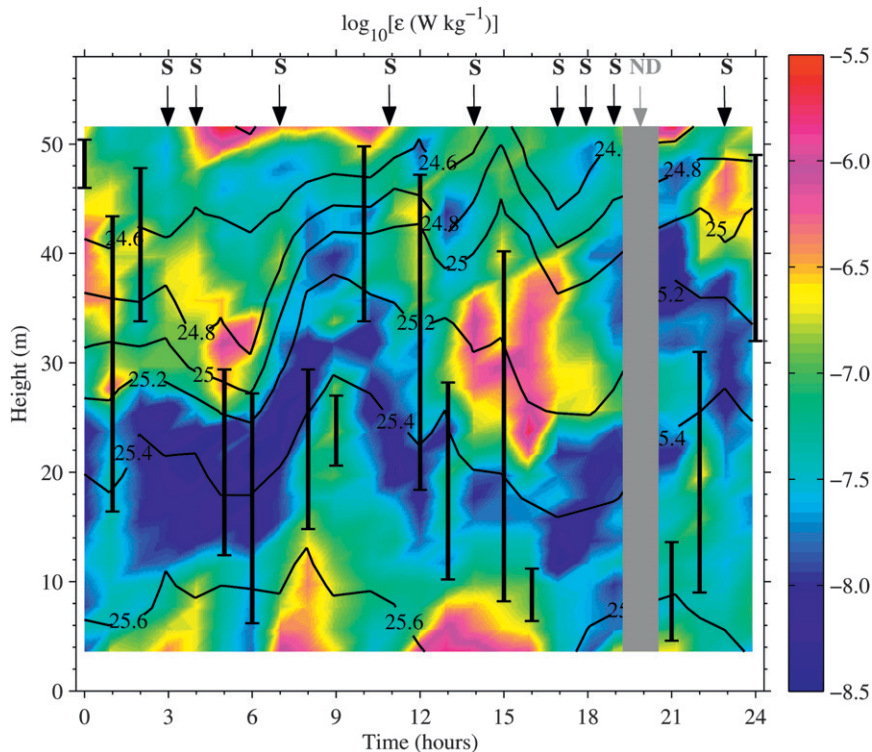


FIG. 12. The time variations of  $\varepsilon$  during the 24-h observational period, with isopycnals overlaid (same as Fig. 4c). The height ranges in which the integrated dissipation rates  $E$  are calculated during the 15 hourly periods are shown as the thick solid bars. The 10 hourly periods in which the flows are stable are marked as “S” and solid arrows. No data available for hour 20; the plot is shaded and marked as “ND” and gray solid arrow.

that is,  $\Phi_c < 0$  and  $|\Phi_c|$  is not much less than unity. This provides further examples in support of the conclusion of Thorpe and Liu (2009) that naturally occurring stratified flows are not, in general, in a marginal state.

- 4) A relation between the estimated growth rate of the fastest growing disturbances to the flow and the observed rates of dissipation of turbulent kinetic energy per unit mass has been devised, that is, Eq. (2). This has, however, an uncertainty factor of about 3 for the dissipation rates and does not provide a simple means to estimate dissipation because of the need to solve the T-G equation. Furthermore, as shown in Fig. 12, the regions where dissipation is greatest do not always correspond to those where the most unstable disturbances have their greatest amplitude.

The results provide some support for the hypothesis that a mechanistic link exists between the measured rates of dissipation of turbulence kinetic energy and the dynamic instability of the flow, but it does not presently lead to a useful means of predicting dissipation rates. A more extensive dataset might reveal whether the in-

stability of the flow at an earlier time determines subsequent dissipation rates.

*Acknowledgments.* The work presented in this paper was conducted during my visit to the School of Ocean Sciences, Bangor University (UK), which was financially supported by the China Scholarship Council. The work was partly supported by the Major State Program of China for Basic Research (Grant 2006CB400602). Prof. Steve Thorpe (Bangor University) has provided many constructive suggestions throughout the whole process of the work and substantially improved the presentation of the paper, for which I am most grateful. The data used in this study were kindly made available by Dr. Tom Rippeth (Bangor University) and were partly analyzed through the NERC Standard Grant NE/F002858. I gratefully acknowledge Dr. Rippeth for his generosity and permission to use the data. I benefited from discussions with Drs. Bill Smyth (Oregon State University, USA) and Andy Hogg (The Australian National University, Australia) in the early stage of the work. I would like to thank the two anonymous reviewers for their critical comments and useful recommendations.

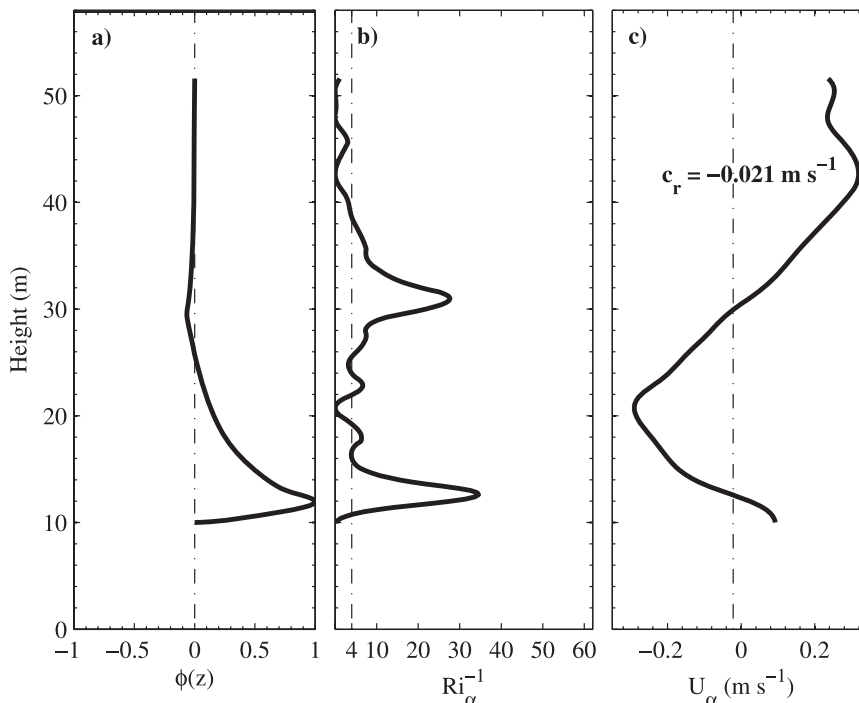


FIG. A1. The (a) normalized amplitude of the streamfunction  $\phi(z)$  of the fastest growing disturbance, (b) inverse directional gradient Richardson number  $Ri_\alpha^{-1}$ , and (c) velocity component in direction  $\alpha = -60^\circ$  of hour-15 flow for case B.

## APPENDIX

### The Sensitivity of the Results to the Location of the Boundaries and the Growth of Local Disturbances

We examine here the sensitivity of the results to the choice for the location of the lower and upper boundaries in solving the T-G equation by conducting three controlled experiments to the hour-15 flow: case A—moving the upper boundary (from  $z = 51.6$  m) to  $z = 44$  m, keeping the lower boundary at  $z = 3.6$  m; case B—moving the lower boundary (from  $z = 3.6$  m) to  $z = 10$  m, keeping the upper boundary at  $z = 51.6$  m; case C—the lower boundary to  $z = 16$  m, keeping the upper boundary at  $z = 51.6$  m. The velocity component in direction  $\alpha = -60^\circ$  of the hour-15 flow and corresponding buoyancy frequency are used in these experiments. As shown in Fig. 10b, in case A, the vertical range of the flow is narrowed by removing a region of high  $Ri_\alpha$  ( $>0.25$ ), whereas in cases B and C, the lower one and two minimum  $Ri_\alpha$  regions are removed, respectively, by moving the lower boundary to  $z = 10$  and  $16$  m.

It is found that, for case A, there are no apparent changes in the results, confirming that imposing the boundary condition of zero velocity at  $z = 51.6$  m is

appropriate for the stability analysis of the flow. As for case B (Fig. A1), by moving the lower boundary to  $z = 10$  m, we remove the near-bottom low  $Ri_\alpha$  region centered at  $z = 5.6$  m. The greatest growth rate is found to decrease from  $1.31 \times 10^{-2}$  to  $0.80 \times 10^{-2} \text{ s}^{-1}$ , and the phase speed is  $-0.021 \text{ m s}^{-1}$ , matching  $U_\alpha$  at  $z = 12.6$  and  $30.0$  m. The fastest growing disturbance keeps a second-mode vertical structure, but the maximum amplitude of the streamfunction moves to a height of  $12.0$  m, close to the level of the minimum  $Ri_\alpha$  (cf. Figs. A1a,b). The second maxima of the amplitude of the streamfunction is now at  $z = 29.6$  m, in the vicinity of the level of a local minimum  $Ri_\alpha$ . The wavelength of the fastest growing disturbance is  $28.25$  m. For case C (Fig. A2), only one low  $Ri_\alpha$  region, at  $z = 31$  m, is left. The fastest growing disturbance has a first-mode vertical structure, with the maxima locating at  $z = 29.2$  m, in the close vicinity of the level of the minimum  $Ri_\alpha$ . The greatest growth rate is  $0.47 \times 10^{-2} \text{ s}^{-1}$ , corresponding to an  $e$ -folding period of  $211.9$  s. The wavelength of the fastest growing disturbance is  $60.5$  m,<sup>4</sup> and the phase speed is  $0.0097 \text{ m s}^{-1}$ , matching  $U_\alpha$  at  $z = 30.8$  m.

<sup>4</sup> A wavelength range of  $0.5$ – $120$  m, with an increment of  $0.5$  m, was adopted in the calculation.

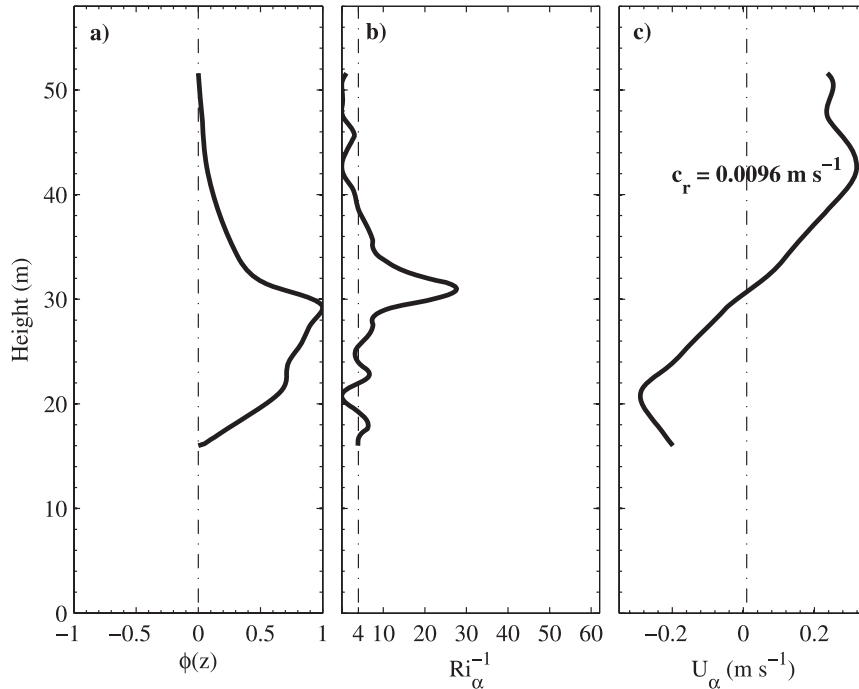


FIG. A2. Same as Fig. A1, but for case C.

It is concluded from the experiments that 1) the results are not sensitive to the precise position of the upper boundary given that the near-upper boundary layer is occupied by a region of high  $Ri_\alpha$  ( $>0.25$ ); 2) the instability of the flow is mainly attributed to the three low  $Ri_\alpha$  regions, centered (i.e., the levels of the local mini-

mum  $Ri_\alpha$ ) at  $z = 5.6, 12.6,$  and  $31$  m, respectively, and the region in which the amplitudes of the streamfunction of the fastest growing disturbances are significant occurs in the vicinity of the lower two low  $Ri_\alpha$  regions. However, the lower two of the low  $Ri_\alpha$  zones are within the bottom boundary layer (see Fig. 6e), where the

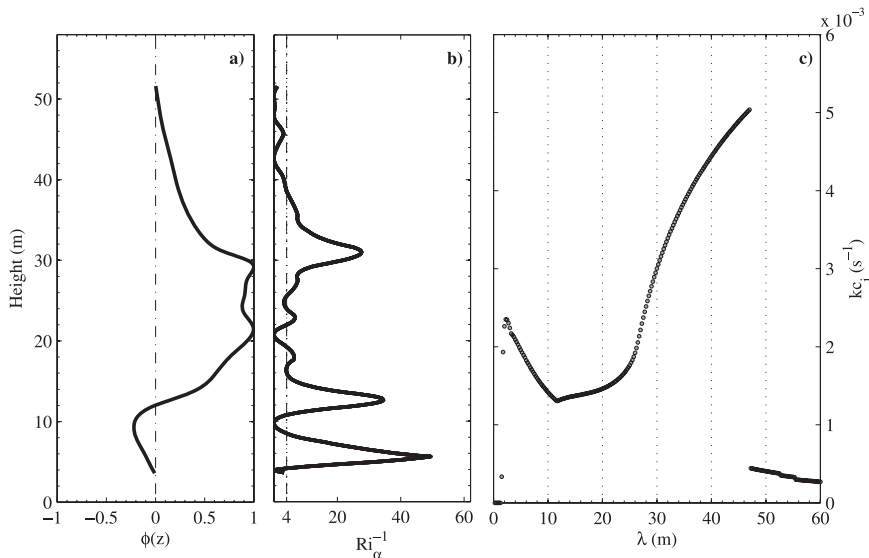


FIG. A3. Results for the disturbances with the maximum amplitude of the streamfunction in the vicinity of the upper local minimum  $Ri_\alpha$  (maximum  $Ri_\alpha^{-1}$ ) for hour 15 with  $\alpha = -60^\circ$ : (a) the normalized amplitude of the streamfunction  $\phi(z)$  of the fastest growing disturbances, (b) the inverse directional gradient Richardson number  $Ri_\alpha^{-1}$ , and (c) the growth rate  $kc_i$  vs wavelength  $\lambda$ .

turbulence is significantly generated by the shear stress close to the bottom. Because the objective is to examine the relation between Kelvin–Helmholtz instability and turbulence, it is not appropriate to include this near-bed region. It can be seen from Fig. A2 that the maximum amplitude of the streamfunction of the fastest growing disturbances would be near the upper local minimum  $Ri_\alpha$  near the pycnocline, where the production of the turbulent kinetic energy results from the local dynamic instability, if we remove the lower two low  $Ri_\alpha$  regions.

We may ask now, is there any growing disturbance with a maximum amplitude of the streamfunction in the vicinity of the upper local minimum  $Ri_\alpha$  for the hour-15 flow? This is important because we should like to relate the greatest growth rate of the disturbances to the observed turbulent dissipation rate within the region where instability is predicted to occur, that is, where the normalized amplitude of the streamfunction is large. The results of our examinations are shown in Fig. A3. The greatest growth rate of the disturbances that have a maximum amplitude of the streamfunction in the vicinity of the upper local minimum  $Ri_\alpha$  is  $0.50 \times 10^{-2} \text{ s}^{-1}$ . The fastest growing disturbance has a second-mode vertical structure, with the maximum amplitude of the streamfunction at a height of 29.6 m and the second maxima at 9.2 m. The wavelength of the fastest growing disturbance is 47.0 m, and the phase speed is  $0.0156 \text{ m s}^{-1}$ , matching  $U_\alpha$  at  $z = 6.0, 12.2, \text{ and } 30.8 \text{ m}$  (see Fig. 10c).

#### REFERENCES

- Gregg, M. C., 1989: Scaling turbulent dissipation in the thermocline. *J. Geophys. Res.*, **94**, 9686–9698.
- Hazel, P., 1972: Numerical studies of the stability of inviscid stratified shear flows. *J. Fluid Mech.*, **51**, 39–61.
- Howard, L. N., 1961: Note on a paper by John W. Miles. *J. Fluid Mech.*, **10**, 509–512.
- Kunze, E. A., A. J. Willams III, and M. G. Briscoe, 1990: Observations of shear and vertical stability from a neutrally buoyant float. *J. Geophys. Res.*, **95** (C10), 18 127–18 142.
- Liu, Z., H. Wei, I. D. Lozovatsky, and H. J. S. Fernando, 2009: Late summer stratification, internal waves, and turbulence in the Yellow Sea. *J. Mar. Syst.*, **77**, 459–472.
- MacKinnon, J. A., and M. C. Gregg, 2003: Mixing on the later-summer New England shelf—Solibores, shear, and stratification. *J. Phys. Oceanogr.*, **33**, 1476–1492.
- , and —, 2005: Spring mixing: Turbulence and internal waves during restratification on the New England shelf. *J. Phys. Oceanogr.*, **35**, 2425–2443.
- Miles, J. W., 1961: On the stability of heterogeneous shear flows. *J. Fluid Mech.*, **10**, 496–508.
- Monserrat, S., and A. J. Thorpe, 1996: Use of ducting theory in an observed case of gravity waves. *J. Atmos. Sci.*, **53**, 1724–1736.
- Palmer, M. R., T. P. Rippeth, and J. H. Simpson, 2008: An investigation of internal mixing in a seasonally stratified shelf sea. *J. Geophys. Res.*, **113**, C12005, doi:10.1029/2007JC004531.
- Polzin, K. L., J. M. Toole, and R. W. Schmitt, 1995: Finescale parameterizations of turbulent dissipation. *J. Phys. Oceanogr.*, **25**, 306–328.
- Rippeth, T. P., and M. E. Inall, 2002: Observations of the internal tide and associated mixing across the Malin Shelf. *J. Geophys. Res.*, **107**, 3028, doi:10.1029/2000JC000761.
- Simpson, J. H., W. R. Crawford, T. P. Rippeth, A. R. Campbell, and J. V. S. Cheok, 1996: The vertical structure of turbulent dissipation in shelf seas. *J. Phys. Oceanogr.*, **26**, 1579–1590.
- Sun, C. J., W. D. Smyth, and J. N. Moum, 1998: Dynamic instability of stratified shear flow in the upper equatorial Pacific. *J. Geophys. Res.*, **103** (C5), 10 323–10 337.
- Sundfjord, A., I. Fer, Y. Kasajima, and H. Svendsen, 2007: Observations of turbulent mixing and hydrography in the marginal ice zone of the Barents Sea. *J. Geophys. Res.*, **112**, C05008, doi:10.1029/2006JC003524.
- Thorpe, S. A., 1999: On the breaking of internal waves in the ocean. *J. Phys. Oceanogr.*, **29**, 2433–2441.
- , and R. Jiang, 1998: Estimating internal waves and diapycnal mixing from conventional mooring data in a lake. *Limnol. Oceanogr.*, **43**, 936–945.
- , and Z. Liu, 2009: Marginal instability? *J. Phys. Oceanogr.*, **39**, 2373–2381.